International Journal of Remote Sensing

ISSN: 0143-1161 (Print) 1366-5901 (Online) Journal homepage: http://www.tandfonline.com/loi/tres20

Assessment of image processing techniques and ASTER SWIR data for the delineation of evaporates and carbonate outcrops along the Salt Lake Fault, Turkey

Aziz Özyavaş

To cite this article: Aziz Özyavaş (2016) Assessment of image processing techniques and ASTER SWIR data for the delineation of evaporates and carbonate outcrops along the Salt Lake Fault, Turkey, International Journal of Remote Sensing, 37:4, 770-781, DOI: 10.1080/2150704X.2015.1130873

To link to this article: http://dx.doi.org/10.1080/2150704X.2015.1130873

Published online: 10 Feb 2016.

Submit your article to this journal

Article views: 17

View related articles

View Crossmark data

Full Terms & Conditions of access and use can be found at
http://www.tandfonline.com/action/journalInformation?journalCode=tres20

Download by: [University of York] **Date:** 17 February 2016, At: 08:03

INTERNATIONAL JOURNAL OF REMOTE SENSING, 2016
VOL. 37, NO. 4, 770–781
http://dx.doi.org/10.1080/2150704X.2015.1130873

Taylor & Francis
Taylor & Francis Group

Assessment of image processing techniques and ASTER SWIR data for the delineation of evaporates and carbonate outcrops along the Salt Lake Fault, Turkey

Aziz Özyavaş

Department of Geological Engineering, Kocaeli University, Kocaeli, Turkey

ABSTRACT

The Advanced Spaceborne Thermal Emission and Reflection Radiometer (ASTER) multispectral sensor allows a variety of minerals to be diagnosed with the availability of six shortwave infrared (SWIR) bands. The study area located in a semi-arid region in central Turkey was flanked by the Salt Lake Fault in the west. ASTER SWIR bands and the adopted image processing techniques such as decorrelation stretch, band ratio, and feature-oriented principle component selection (FPCS) were applied for mapping both gypsum and carbonate rocks in the study area. Initially, the application of the decorrelation stretch method with a novel band combination successfully delineated the gypsum and carbonate outcrops. In addition to that, the principle component 4 (PC4) image obtained from the FPCS technique applied to a new band selection of ASTER data distinguished explicitly the carbonate outcrops. The resultant images, consistent with the geologic map of the study area, were compared with another and demonstrated that the gypsum and carbonate rocks were clearly identifiable. In addition to that, quantitative analyses of parallelepiped supervised classification images, band 9/band 8 ratio, and PC4 images in particular, yielded very compatible results.

ARTICLE HISTORY
Received 16 February 2015
Accepted 1 December 2015

Downloaded by [University of York] at 08:03 17 February 2016

1. Introduction

The Advanced Spaceborne Thermal Emission and Reflection Radiometer (ASTER), launched in December 1999, is a multispectral imager aboard the Earth Observing System (EOS) Terra platform (Yamaguchi and Naito 2003). Since the narrow ASTER shortwave infrared (SWIR) bands allow various minerals to be identified, multispectral ASTER images have been widely and successfully employed by several workers to map lithologies, ore deposits, minerals, and alteration products in various geologic settings (Rowan and Mars 2003; Yamaguchi and Naito 2003; Mars and Rowan 2010; Rockwell and Hofstra 2008; Gabr, Ghulam, and Kusky 2010; Rajendran et al. 2013; Oztan and Suzen 2011).

The study area is located to the east of the Salt Lake along the southern part of the Salt Lake Fault in central Turkey (Figure 1). The subset of the ASTER scene selected for this

CONTACT Aziz Özyavaş aziz.ozyavas@kocaeli.edu.tr Department of Geological Engineering, Kocaeli University, Kocaeli, Turkey.

© 2016 Taylor & Francis

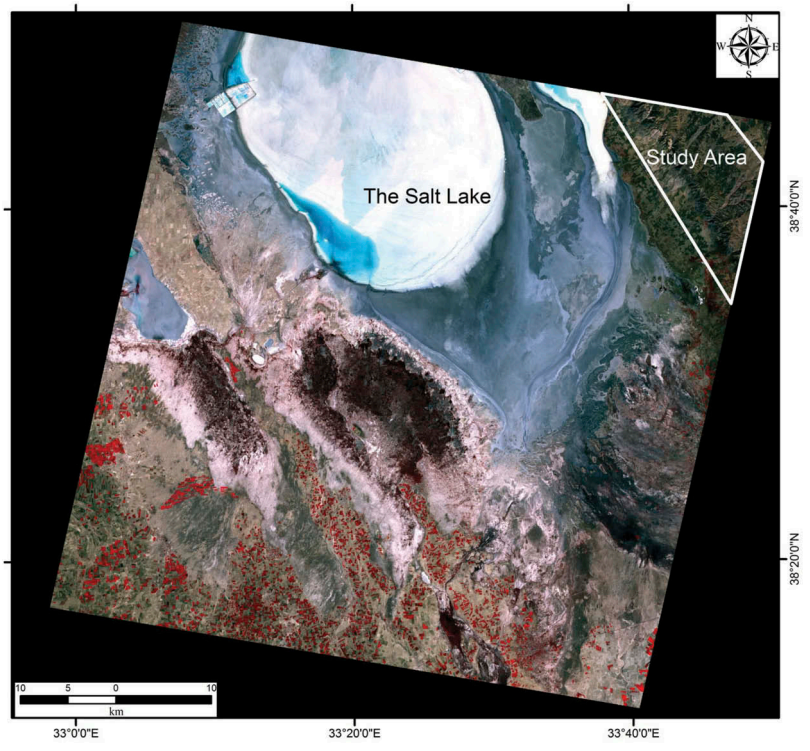

Figure 1. ASTER false-colour-composite image 3, 2, 1 (Red-band 3, Green-band 2, Blue-band 1) showing the location of the study area in central Turkey.

research includes evaporates and detrital and carbonate rocks (Figure 2). The main objective of this article is to demonstrate the capability of the applied image processing methods along with the ASTER SWIR bands to diagnose both evaporates and carbonate rocks.

2. Geological settings

The study area is underlain by magmatic and metamorphic rocks and ophiolites known as the Central Anatolian Crystalline Complex (CACC) or Kırşehir Massif of Palaeozoic and Mesozoic age (Göncüoğlu et al. 1991). The CACC is composed mainly of granodiorites along with orderly pilings of middle Anatolian metamorphic rocks, metamorphosed and deformed ophiolites, and ophiolites related to intra-oceanic subduction zones (Göncüoğlu et al. 1991; Yalınız, Göncüoğlu, and Özkan-Altıner 2000). Terrestrial conditions prevailed succeeding the marine conditions from the late Eocene to the Oligocene, causing the precipitation of thick evaporate deposits in ephemeral lakes (Arıkan 1975). While Oligocene and lower Miocene evaporates mainly crop out along the Salt Lake Fault in the north of the study area, detrital and carbonate rocks of the upper Senonian and Palaeocene are exposed all the way along the Salt Lake Fault (Figure 2).

Downloaded by [University of York] at 08:03 17 February 2016

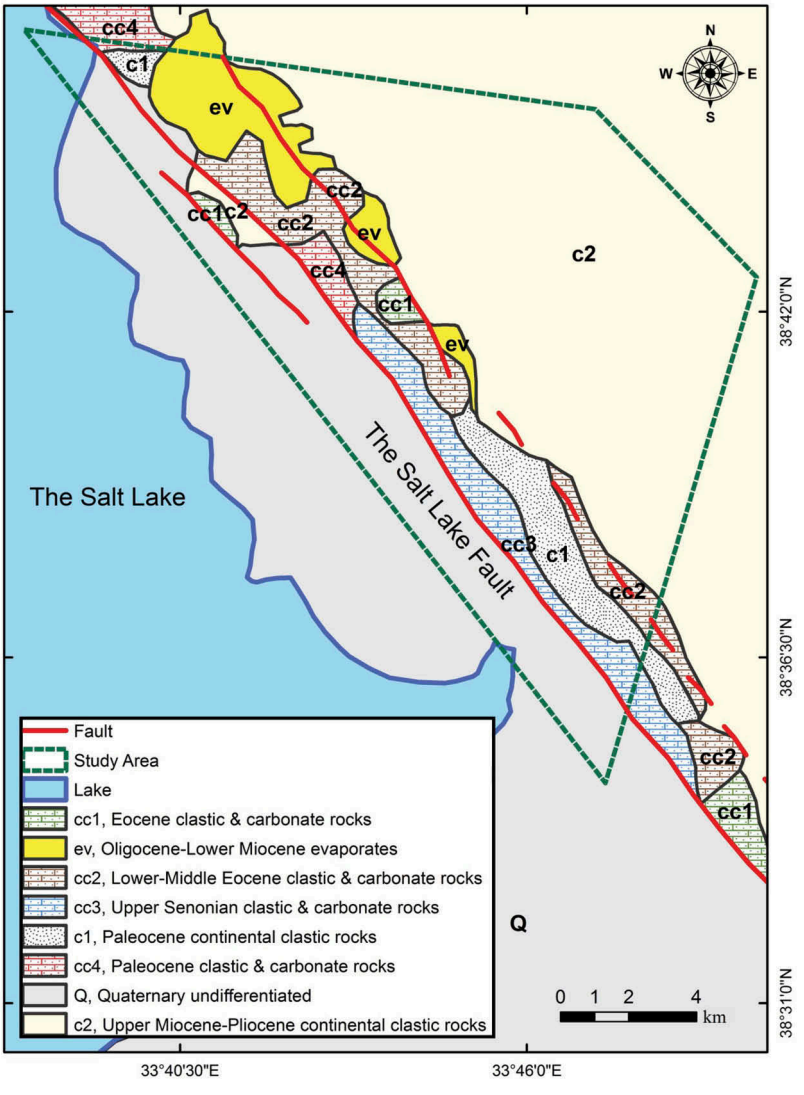

Figure 2. Generalized geologic map of the study area (modified from the Directorate of Mineral Research and Exploration). The study area is shown as a dashed trapezoid.

3. Data

The ASTER data was utilized in this work for its spectral characteristics in the SWIR region and relatively inexpensive cost. The ASTER level 1B registered radiance at sensor data set acquired on October 8, 2005 covers the study area. Environment for Visualizing Images (ENVI) 5.0 and Arc geographic information system (GIS) 9.3 from Environmental Systems Research Institute (ESRI) were employed for image processing and analyses. The geologic map of the study area was digitized and modified from the data provided by the Directorate of Mineral Research and Exploration (MTA) in Ankara, Turkey (Figure 2). The reflectance spectra of the gypsum and calcite in Figure 3 were derived from the USGS spectral library.

Downloaded by [University of York] at 08:03 17 February 2016

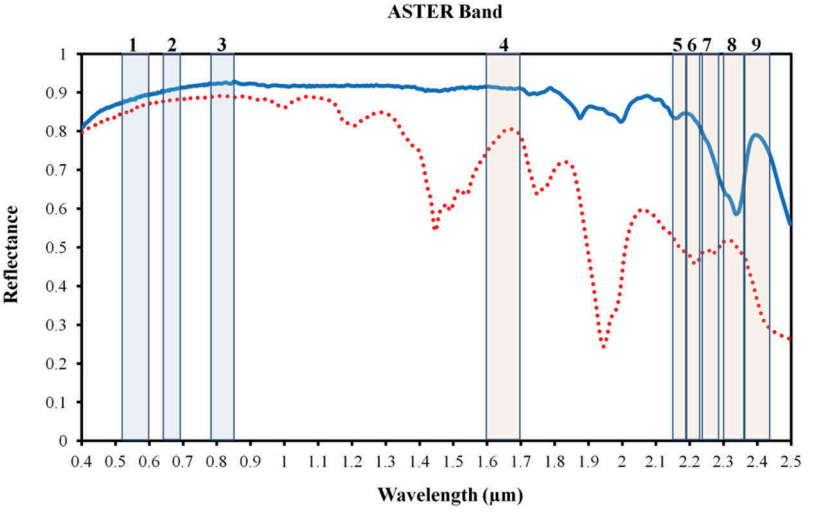

Figure 3. The locations and bandwidths of ASTER SWIR bands labelled from 4 through 9. The reflectance spectra of gypsum (dotted line) and calcite (solid line) came from a spectral library prepared by USGS.

4. Methodology

As a first step, ASTER data was georeferenced and an atmospheric correction algorithm, the Fast Line-of-sight Atmospheric Analysis of the Spectral Hypercubes (FLAASH), was applied to SWIR bands to remove the spectral effects of aerosols and water vapour from the data. After preprocessing of the ASTER data set, the SWIR spectral reflectance data were analysed by using a series of band ratio images. Band ratio is a robust and simple technique to enhance the spectral contrast of various minerals and to reduce the variations in spectral reflectance caused by topography or changes in sunlight illumination conditions (Rowan and Mars 2003). The Principle Component Analysis (PCA) technique applied to ASTER SWIR data in this work is a simple, fast and robust technique that produces uncorrelated output bands and has been used widely to map minerals for decades (Crosta et al. 2003). Gypsum and carbonate rock discrimination was made with ASTER data transformation using the decorrelation stretch (DC) technique, which enhances the subtle variations by removing the inter-band correlation (Rowan and Mars 2003). The supervised classification technique used in this study was the parallelepiped approach which clusters the image pixels into classes corresponding to the defined training classes (Richards 1999). A flowchart of the data process is illustrated in Figure 4.

5. Results and Discussion

The SWIR region of the electromagnetic spectrum is very useful for differentiating particularly clay minerals, carbonates, sulphates, and other minerals based on the spectral absorption features (Hunt 1977). As both gypsum and calcite have diagnostic spectral features in SWIR wavelengths of the electromagnetic spectrum, ASTER bands

Downloaded by [University of York] at 08:03 17 February 2016

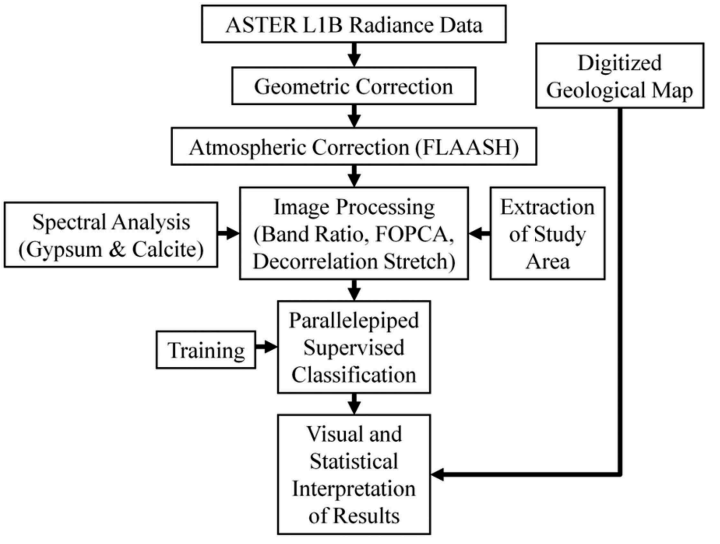

Figure 4. Workflow of data and procedures used for lithologic information retrieval.

corresponding to this range from band 4 through 9 (Figure 3) were utilized in image analyses in this work.

5.1. *Decorrelation stretch*

Herein a new band combination was used to delineate gypsum deposits as well as carbonate rocks using the decorrelation stretch method. Several RGB band combinations of decorrelation stretch images were produced by selecting ASTER bands where both gypsum and carbonates possess diagnostic high and low reflectance features. As a result, a novel and successful band combination to differentiate gypsum and carbonate rocks from the adjacent rock units was decided to be ASTER bands 4, 8, and 9. The decorrelation stretch (Red-band 4, Green-band 9, Blue-band 8) composite image showed that gypsum as well as soils rich in gypsum appear as magenta in colour (Figure 5a) because gypsum has high spectral reflectance in ASTER band 4 and band 8 and absorbs electromagnetic energy strongly in band 9. On the other hand, since the carbonates have a characteristic absorption feature in ASTER band 8 and high spectral reflectance in band 9, green colour is very likely to represent carbonate rocks in the decorrelation stretch composite image. The classification of the decorrelation stretch image is shown in Figure 5b for comparison.

5.2. *Band ratio*

Gypsum has high spectral reflectance corresponding to the wavelengths of ASTER band 4 and band 8 and absorbs in band 6 and band 9. Evaporate outcrops were studied using several ASTER band ratios and the band 4/band 9 ratio image was decided to be the most successful band ratio image (Oztan and Suzen 2011). Band ratios 4/6 (band 4/band 6), 4/9 (band 4/band 9), 8/6 (band 8/band 6), 8/9 (band 8/band

Downloaded by [University of York] at 08:03 17 February 2016

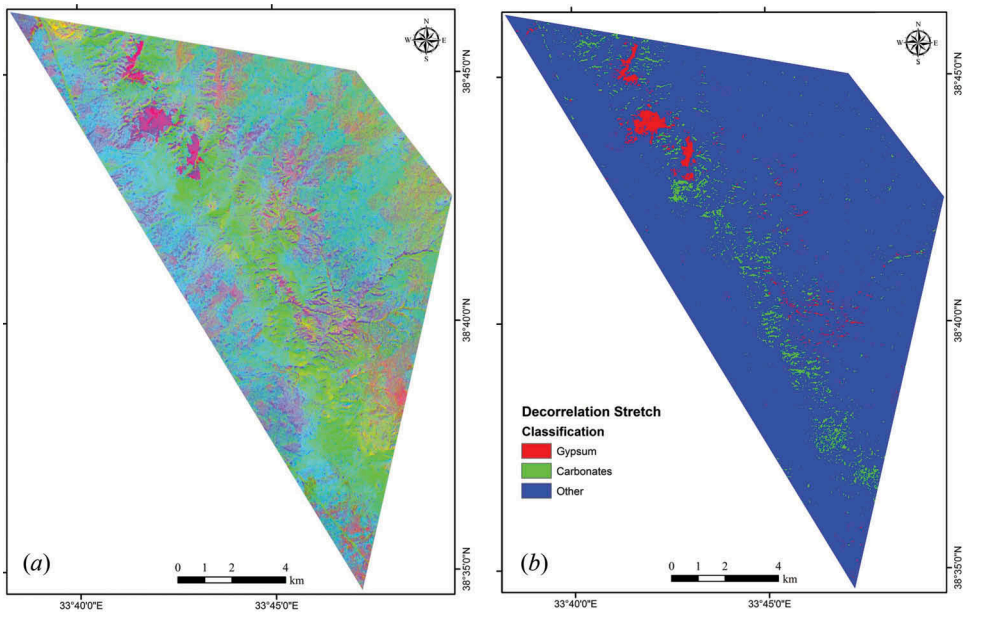

Figure 5. (a) The decorrelation stretch colour composite image (Red-band 4, Green-band 9, Blue-band 8). Gypsum outcrops at the northwestern part of the study area and gypsum-rich soils are shown as magenta in colour. Carbonate rocks extending from the southeast to the northwest like a ribbon are represented by the green colour. (b) The classified image of decorrelation stretch colour composite showing gypsum in red, carbonate rocks in green, and other lithologies in blue.

9), (4 + 8)/9 ((band 4 + band 8)/band 9), and (4 + 8)/6 ((band 4 + band 8)/band 6) for gypsum were selected so that gypsum appeared as bright pixels in band ratio images. Although, all of the band ratio images of gypsum clearly distinguished gypsum from other lithologies, the band ratio ((band 4 + band 8)/band 6) resulted in the largest contrast between gypsum outcrops and surrounding lithologies (Figure 6). The range of the gypsum outcrop values was around from 2.543 to 3.286 (Figure 6). On the other hand, calcite has a diagnostic high reflectance and an absorption feature in wavelengths corresponding to ASTER band 9 and band 8, respectively (Mars and Rowan 2010). As a result, carbonates appeared as bright pixels in a band 9/band 8 ratio image where the gypsum deposits represented dark pixels due to the low and high reflectance in band 9 and band 8, respectively (Figure 7a). While the value of pixels representing gypsum ranged approximately from 0.672 to 0.823, carbonate rocks possessed values between about 1.113 and 1.496 (Figure 7a). The band 9/band 8 ratio image appeared to be consistent with the classification image (Figure 7b).

5.3. *PCA*

Crosta and Moore (1989) developed a method, called FPCS, by selecting particular principle component (PC) images that characterize spectral responses of target minerals based on the values of an eigenvector matrix. Oztan and Suzen (2011) applied PCA to four ASTER bands (4, 6, 8, and 9) to study evaporates on the basis of the Crosta

Downloaded by [University of York] at 08:03 17 February 2016

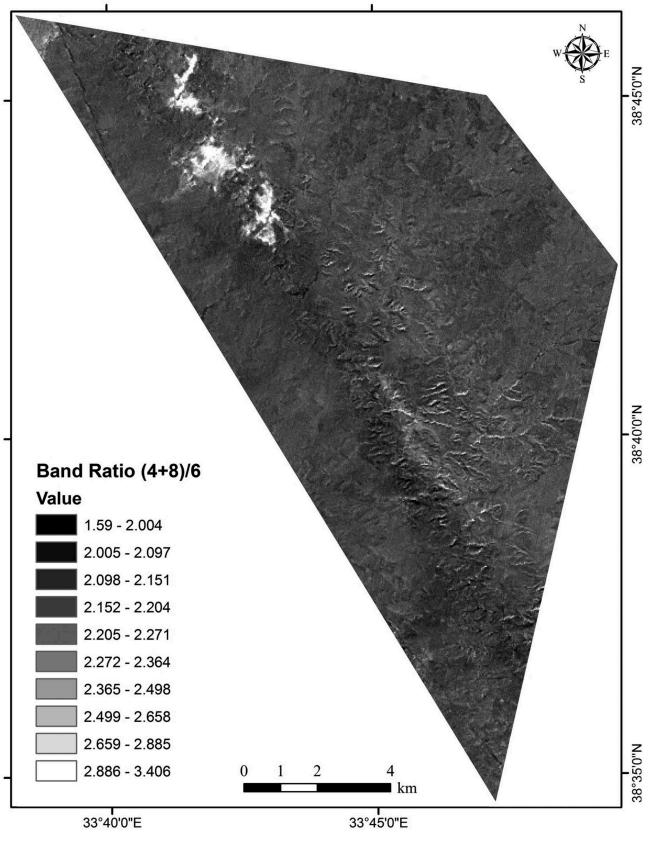

Figure 6. ASTER band (4 + 8)/band 6 ratio image of the study area with bright pixels at the northwest indicating the gypsum deposits.

technique proposed by Loughlin (1991) and PC3 was selected as the most appropriate image to clearly display gypsum deposits. In this work, the ASTER SWIR bands 4, 6, 8, and 9 were selected in the FPCS technique to delineate gypsum deposits. The selection of ASTER SWIR bands for FPCS analysis were based on the position of characteristic spectral signatures of gypsum and calcite where both have high and low spectral reflectance values. To my knowledge, ASTER SWIR 4, 6, 8, and 9 band selection for carbonates has been used for the first time in the FPCS method. The eigenvector statistics of ASTER SWIR bands were examined to determine the most useful PC which contained the information of gypsum and carbonates (Table 1). Loughlin's (1991) proposed that the PC having the highest eigenvector loadings from the selected bands contains the spectral information for the target material. On the basis of Loughlin's (1991) suggestion all of the PCs were analysed and discussed. First of all, PC4 had a high and positive loading (0.625) from ASTER band 8 and a high and negative loading (−0.777) from band 9. In addition to that, the loadings of PC4 from band 4 (0.030) and 6 (0.065) exhibited considerably lower values compared to band 8 and band 9, so their contributions to gypsum and carbonates can be neglected (Table 1). Therefore, in Figure 8a while bright pixels in PC4 were very likely to represent gypsum, pixels that appeared as dark areas indicated carbonate rocks. Bright pixels indicating gypsum deposits displayed values

Downloaded by [University of York] at 08:03 17 February 2016

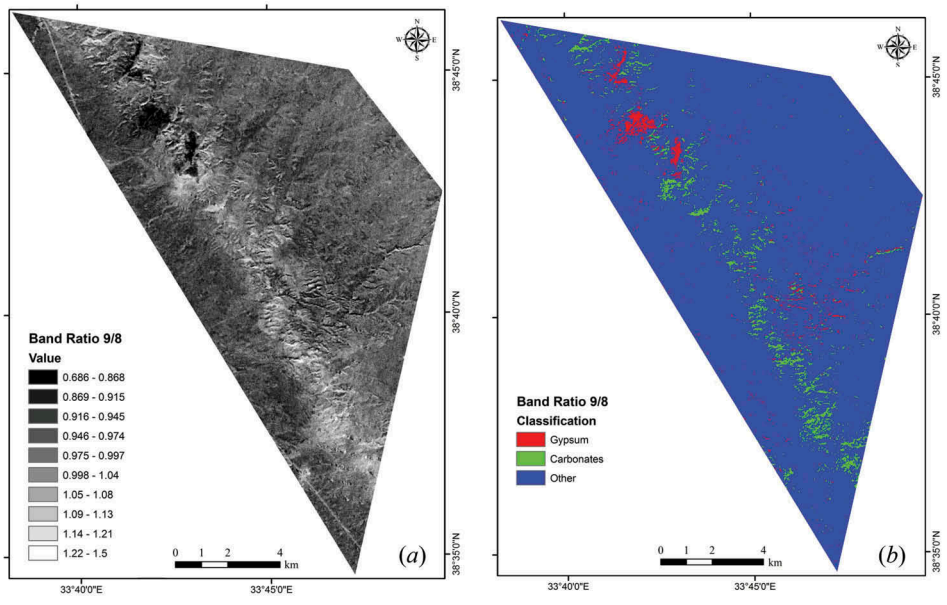

Figure 7. (a) A band of carbonate rocks all the way from southeast to the northwest represented by bright pixels in contrast to the gypsum deposits indicated by dark pixels at the northwest of the study area in an ASTER band 9/band 8 ratio image. (b) The classification of ASTER band 9/band 8 ratio image, gypsum represented by red, carbonate rocks by green and other lithologies by blue colour.

Table 1. Eigenvector loadings for the selected ASTER bands 4, 6, 8, and 9 used to determine the spectral response of gypsum and carbonate rocks. While PC2 and PC4 were found to be very useful to identify gypsum and carbonates, PC1 and PC3 cannot delineate the target materials.

	PC1	PC2	PC3	PC4
Band 4	0.642	0.698	0.317	0.030
Band 6	0.494	−0.064	−0.865	0.065
Band 8	0.423	−0.566	0.331	0.625
Band 9	0.407	−0.434	0.206	−0.777

between 0.0241and 0.059 and the values of carbonate rocks shown as dark pixels ranged from −0.054 to −0.024 (Figure 8a). Gypsum and carbonate outcrops in the PC4 image matched well with those in the classification image (Figure 8b). As for PC2, ASTER bands 6, 8, and 9 had high and negative loadings (−0.064, −0.566, −0.434, respectively) except for the band 4 which had a high and positive loading (0.698). Thus, PC2 was useful to display only gypsum deposits as bright pixels (values ranging from 0.030 to 0.114 in Figure 9), which was consistent with the result of the PC4 image. On the other hand, all of the eigenvector loadings for PC1 were high and positive (Table 1), therefore the differentiation of gypsum and carbonates from other rocks was not possible. Gypsum and carbonates in the PC3 image cannot be detected because eigenvector loadings from ASTER bands 4, 8, and 9 were positive and similar values. As a result, while PC4 and PC2 images were suitable for differentiating gypsum and carbonate rocks from other lithologies, PC1 and PC3 cannot be used to display the target outcrops.

Downloaded by [University of York] at 08:03 17 February 2016

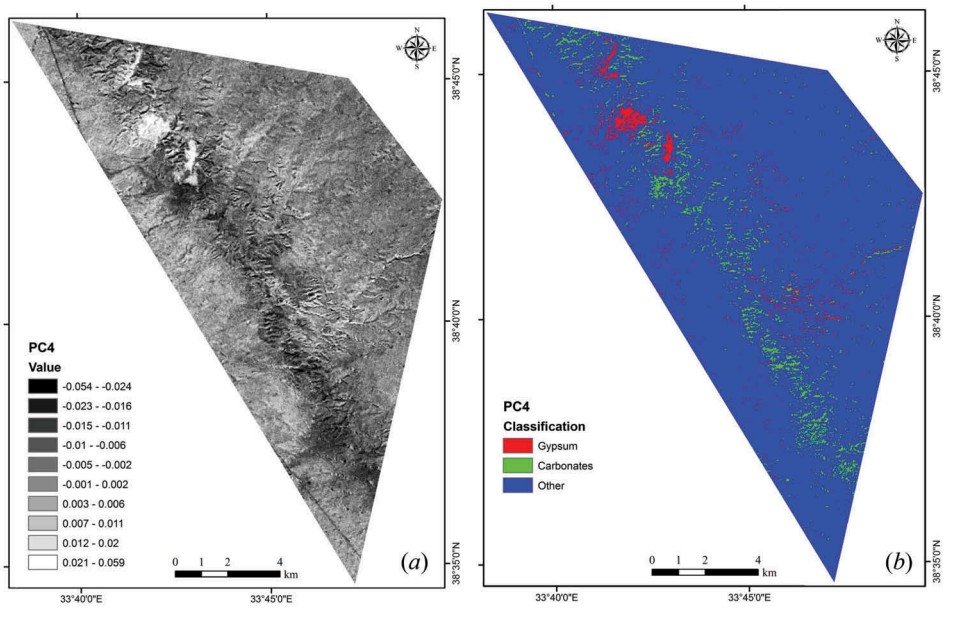

Figure 8. (a) Carbonate rocks and gypsum shown as dark and bright pixels respectively in the PC4 image of the study area. (b) The classification of the PC4 image indicating gypsum as red, carbonate rocks as green, and other lithologies as blue in colour.

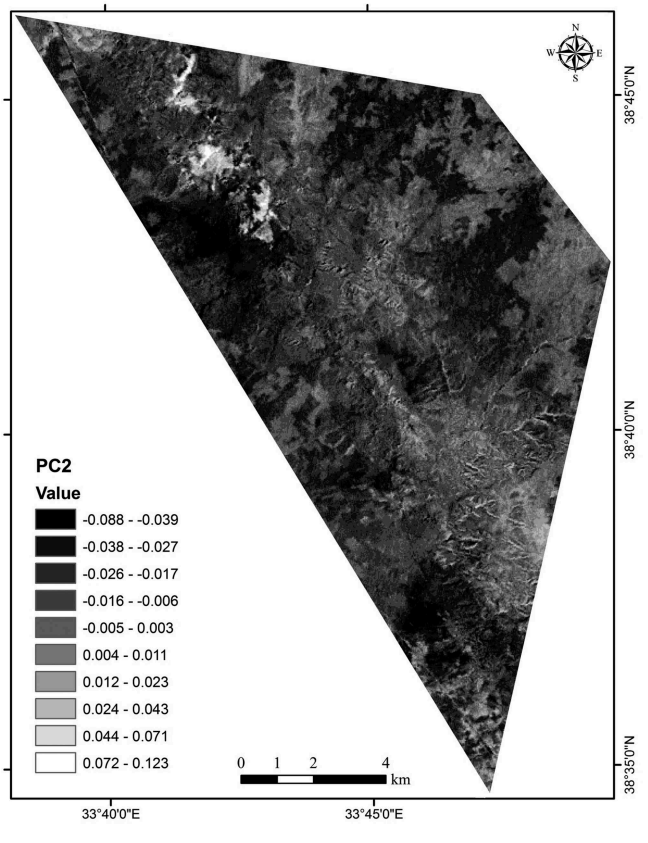

Figure 9. Gypsum deposits indicated by bright pixels in the PC2 image of the study area.

Downloaded by [University of York] at 08:03 17 February 2016

Downloaded by [University of York] at 08:03 17 February 2016

Table 2. Classification image difference statistics results. While the initial state (columns) indicates the first image, the final stage (rows) indicates the second image. Reciprocal classification image pairs used to calculate statistics for the band 9/band 8 ratio, PC4, and decorrelation stretch classification images.

		Initial State				Initial State	
	1	Gypsum (Band Ratio 9/8) Pixel Counts/Percentages	Carbonates (Band Ratio 9/8) Pixel Counts/Percentages		**2**	Gypsum (PC4) Pixel Counts/Percentages	Carbonates (PC4) Pixel Counts/Percentages
Final State	Gypsum (PC4)	2623/85.2	0/0	Final State	Gypsum (Band Ratio 9/8)	2623/85.1	0/0
	Carbonates (PC4)	0/0	5589/80.5		Carbonates (Band Ratio 9/8)	0/0	5589/77.8
	Other (PC4)	457/14.8	1352/19.5		Other (Band Ratio 9/8)	461/14.9	1594/22.2
	Class Total	3080/100	6941/100		Class Total	3084/100	7183/100
	Class Changes	457/14.8	1352/19.5		Class Changes	461/14.9	1594
	Image Difference	4/0.1	242/3.5		Image Difference	4/0.1	242/3.4
	3	Gypsum (PC4) Pixel Counts/Percentages	Carbonates (PC4) Pixel Counts/Percentages		**4**	Gypsum (DS) Pixel Counts/Percentages	Carbonates (DS) Pixel Counts/Percentages
Final State	Gypsum (DS)	2121/68.8	0/0	Final State	Gypsum (PC4)	2121/72.2	0/0
	Carbonates (DS)	0/0	5482/76.3		Carbonates (PC4)	0/0	5482/80.7
	Other (DS)	963/31.2	1701/23.7		Other (PC4)	818/27.8	1310/19.3
	Class Total	3084/100	7183/100		Class Total	2939/100	6792/100
	Class Changes	963/31.2	1701/23.7		Class Changes	818/27.8	1310/19.3
	Image Difference	145/4.7	391/5.4		Image Difference	145/4.9	391/5.8
	5	Gypsum (Band Ratio 9/8) Pixel Counts/Percentages	Carbonates (Band Ratio 9/8) Pixel Counts/Percentages		**6**	Gypsum (DS) Pixel Counts/Percentages	Carbonates (DS) Pixel Counts/Percentages
Final State	Gypsum (DS)	2066/67.1	0/0	Final State	Gypsum (Band Ratio 9/8)	2066/70.3	0/0
	Carbonates (DS)	0/0	4801/69.2		Carbonates (Band Ratio 9/8)	0/0	4801/70.7
	Other (DS)	1014/32.9	2140/30.8		Other (Band Ratio 9/8)	873/29.7	1991/29.3
	Class Total	3080/100	6941/100		Class Total	2939/100	6792/100
	Class Changes	1014/32.9	2140/30.8		Class Changes	873/29.7	1991/29.3
	Image Difference	141/4.6	149/2.1		Image Difference	141/4.8	149/2.2

5.4. *Quantitative analysis*

The classification images of decorrelation stretch (Figure 5b), band 9/band 8 ratio (Figure 7b), and PC4 (Figure 8b) were produced in order to quantify the differences between classification images. The difference of the classification images were computed by subtracting the initial state classification image from the final state classification image. Post-classification change detection statistics was calculated for the band 9/band 8 ratio, PC4, and decorrelation stretch classification images (Table 2). For the sake of examining consistency of the statistics results, each classification image was used to be both initial and final state classification images (i.e. the band 9/band 8 ratio classification image was defined as an initial state image and the PC4 classification image as a final state image in Section 1 and *vice versa* in Section 2 in Table 2). The same procedure was followed for the rest of the classification image pairs. The statistics report included pixel counts and percentages for each class in Table 2 which listed the initial state classes in the columns and the final state classes in the rows. Table 2 points out how pixels in each column (that is, initial state class) were classified in the rows (final state class). For instance, in section 1 of Table 2, 2623 pixels (85.2%) initially classified as gypsum remained gypsum as well in the final state image. On the other hand, while no pixels representing gypsum in the initial state image changed into carbonates, 417 (14.8%) pixels classified as gypsum initially were replaced by other lithologies in the final stage image. Similarly, 5589 pixels (80.5%) initially classified as carbonate rocks remained to be carbonate rocks and 1352 pixels (19.5%) turned into other lithologies in the final stage image in section 1. Section 2 demonstrated similar findings for both gypsum and carbonates. Therefore, gypsum and carbonates exhibited approximately similar values with high percentage in sections 1 and 2. In addition, Class Total, Class Changes, and Image Difference rows in sections 1 and 2 also resulted in consistent values. Furthermore, other pairs of post-classification difference statistics in sections 3 through 6 in Table 2 also displayed similar and high percentage values.

6. Conclusion

The results obtained from this study demonstrated that both the spectral resolution of ASTER data and adopted remote-sensing techniques are capable of identifying and mapping of gypsum and carbonate rocks clearly. One of the contributions of this research was that the decorrelation stretch image derived from a new set of ASTER SWIR bands 4, 8, and 9 successfully delineated gypsum and carbonate outcrops. Moreover, for the first time, the FPCS technique applied to the selected bands of ASTER data (bands 4, 6, 8, and 9) produced the PC4 image which better identified the carbonate rocks. As for the relative accuracy of results, the resultant images of band ratio, PCA, and decorrelation stretch image processing techniques were compared with one another and with the geologic map and found to be correlated remarkably well. Besides, the parallelepiped supervised classification approach was applied to the selected images and quantitatively justified the results.

Downloaded by [University of York] at 08:03 17 February 2016

Disclosure statement

No potential conflict of interest was reported by the author.

Funding

This work was supported by the Kocaeli University.

References

Arıkan, Y. 1975. "Tuz Gölü Havzası'nın Jeolojisi Ve Petrol Imkanları." *MTA Enstitüsü Dergisi* 85: 17–37.

Crosta, A. P., C. R. De Souza Filho, F. Azevedo, and C. Brodie. 2003. "Targeting Key Alteration Minerals in Epithermal Deposits in Patagonia, Argentina, Using ASTER Imagery and Principal Component Analysis." *International Journal of Remote Sensing* 24 (21): 4233–4240. doi:10.1080/0143116031000152291.

Crosta, A. P., and J. M. Moore. 1989. "Enhancement of Landsat Thematic Mapper Imagery for Residual Soil Mapping in SW Minas Gerais State Brazil: A Prospecting Case History in Greenstone Belt Terrain." *Thematic Conference on Remote Sensing for Exploration Geology* 7: 1173–1187.

Gabr, S., A. Ghulam, and T. Kusky. 2010. "Detecting Areas of High-Potential Gold Mineralization Using ASTER Data." *Ore Geology Reviews* 38: 59–69. doi:10.1016/j.oregeorev.2010.05.007.

Göncüoğlu, M. C., G. M. V. Toprak, İ. Kuşçu, A. Erler, and E. Olgun. 1991. "Geology of the Western Part of the Central Anatolian Massif, Part 1: Southern Part." *METU-TPAO Project Report*. Ankara, Turkey.

Hunt, G. 1977. "Spectral Signatures of Particulate Minerals in the Visible and near Infrared." *Geophysics* 42 (3): 501–513. doi:10.1190/1.1440721.

Loughlin, W. 1991. "Principle Component Analysis for Alteration Mapping." *Photogrammetric Engineering and Remote Sensing* 57: 1163–1169.

Mars, J. C., and L. C. Rowan. 2010. "Spectral Assessment of New ASTER SWIR Surface Reflectance Data Products for Spectroscopic Mapping of Rocks and Minerals." *Remote Sensing of Environment* 114: 2011–2025. doi:10.1016/j.rse.2010.04.008.

Oztan, N. S., and M. L. Suzen. 2011. "Mapping Evaporate Minerals by ASTER." *International Journal of Remote Sensing* 32: 1651–1673. doi:10.1080/01431160903586799.

Rajendran, S., S. Nasir, T. M. Kusky, A. Ghulam, S. Gabr, and M. El-Ghali. 2013. "Detection of Hydrothermal Mineralized Zones Associated with Listwaenites in Central Oman Using ASTER Data." *Ore Geology Reviews* 53: 470–488. doi:10.1016/j.oregeorev.2013.02.008.

Richards, J. A. 1999. *Remote Sensing Digital Image Analysis*. Berlin: Springer-Verlag.

Rockwell, B. W., and A. H. Hofstra. 2008. "Identification of Quartz and Carbonate Minerals across Northern Nevada Using ASTER Thermal Infrared Emissivity Data—Implications for Geologic Mapping and Mineral Resource Investigations in Well-Studied and Frontier Areas." *Geosphere* 4: 218–246. doi:10.1130/GES00126.1.

Rowan, L. C., and J. C. Mars. 2003. "Lithologic Mapping in the Mountain Pass, California Area Using Advanced Spaceborne Thermal Emission and Reflection Radiometer (ASTER) Data." *Remote Sensing of Environment* 84: 350–366. doi:10.1016/S0034-4257(02)00127-X.

Yalınız, K., M. C. Göncüoğlu, and S. Özkan-Altıner. 2000. "Formation and Emplacement Ages of the SSZ-Type Neotethyan Ophiolites in Central Anatolia, Turkey: Palaeotectonic Implications." *Geological Journal* 35: 53–68. doi:10.1002/(ISSN)1099-1034.

Yamaguchi, Y., and C. Naito. 2003. "Spectral Indices for Lithologic Discrimination and Mapping by Using the ASTER SWIR Bands." *International Journal of Remote Sensing* 24: 4311–4323. doi:10.1080/01431160110070320.

Downloaded by [University of York] at 08:03 17 February 2016